

CHEMISTRY

A European Journal



Accepted Article

Title: Highly Polarized Coumarin Derivatives Revisited: Solvent-controlled Competition Between Proton Coupled Electron Transfer and Twisted Intramolecular Electron Transfer

Authors: Olaf Morawski, Łukasz Kielesiński, Daniel T Gryko, and Andrzej Sobolewski

This manuscript has been accepted after peer review and appears as an Accepted Article online prior to editing, proofing, and formal publication of the final Version of Record (VoR). This work is currently citable by using the Digital Object Identifier (DOI) given below. The VoR will be published online in Early View as soon as possible and may be different to this Accepted Article as a result of editing. Readers should obtain the VoR from the journal website shown below when it is published to ensure accuracy of information. The authors are responsible for the content of this Accepted Article.

To be cited as: *Chem. Eur. J.* 10.1002/chem.202001079

Link to VoR: <http://dx.doi.org/10.1002/chem.202001079>

Supported by
ACES

WILEY-VCH

FULL PAPER

Highly Polarized Coumarin Derivatives Revisited: Solvent-controlled Competition Between Proton Coupled Electron Transfer and Twisted Intramolecular Electron Transfer

Olaf W. Morawski,^{*[a]} Łukasz Kielesiński,^[a,b] Daniel T. Gryko^{*[b]} and Andrzej L. Sobolewski^{*[a]}Dedicated to Prof. Kyo Han Ahn on occasion of his 65th birthday

- [a] Dr. Olaf W. Morawski, Łukasz Kielesiński, Prof. Andrzej L. Sobolewski
Institute of Physics
Polish Academy of Sciences
Al. Lotników 32/46, 02-668 Warsaw, Poland
E-mail: morawo@ifpan.edu.pl, sobola@ifpan.edu.pl
- [b] Łukasz Kielesiński, Prof. Daniel T. Gryko
Institute of Organic Chemistry
Polish Academy of Sciences
Kasprzaka 44/52, 01-224 Warsaw, Poland
E-mail: dtgryko@icho.edu.pl

Supporting information for this article is given via a link at the end of the document. (Please delete this text if not appropriate)

Abstract: Linking a polarized coumarin unit with an aromatic substituent via an amide bridge results in weak electronic coupling affecting the intramolecular electron transfer (ET) process. As a result of this, interesting solvent-dependent photophysical properties can be observed. In polar solvents, electron transfer in coumarin derivatives of this type induces a mutual twist of electron-donating and electron-accepting molecular units (TICT process) that opens radiationless decay processes (internal conversion). In the dyad with the strongest intramolecular hydrogen bond, the planar form is stabilized so twisting can only occur in highly polar solvents, whereas fast proton coupled electron transfer (PCET process) occurs in non-polar *n*-alkanes. The k_{PCET} rate constant decreases linearly with the fluorescence maximum energy in different solvents. This observation is explained in terms of competition between electron and proton transfer from a highly polarized (~15 D) and fluorescent locally-excited (¹LE) state to a much less polarized (~4 D) charge-transfer (¹CT) state, a unique occurrence. Photophysical measurements performed for a family of related coumarin dyads together with results of quantum-chemical computations give insight into the mechanism of the ET process which is followed by either a TICT or PCET process. Our results reveal that dielectric solvation of the excited state slows down the PCET process, even in non-polar solvents.

Introduction

Photoinduced inter- and intra-molecular electron transfer (ET) processes play an important role in many areas of physics and chemistry, ranging from charge separation in photovoltaics^[1] and photoluminescent sensors and switches,^[2,3] to natural^[4] and artificial^[5] photosynthesis. The theoretical basis for ET processes was originally established in the seminal works of Marcus^[6] and Weller^[7] more than half a century ago. The kinetics and thermodynamics of the ET process is modulated by the electrochemical and excited-state properties of molecular systems, with accompanying structural changes, and is in

competition with radiative and radiationless deactivation processes.^[8-13]

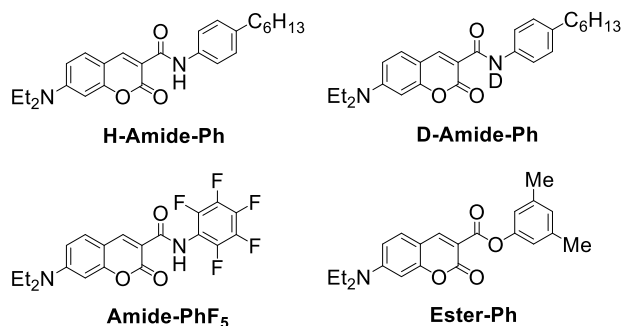
Among the proposed intramolecular structural changes related to the ET process, the twisted intramolecular charge-transfer (TICT) hypothesis of Grabowski et al.^[14] has attracted the most attention (for a review see Ref. [15] and references therein). Another intramolecular structural change related to this phenomenon is the excited-state intramolecular proton transfer (ESIPT) process, introduced originally by Weller decades ago.^[16] Both processes may result in a strongly red-shifted fluorescence^[17-21] and open competing radiationless decay channels.^[22] It has been shown that the radiationless decay channel associated with the ESIPT process involves mutual twisting of the electronically conjugated proton-donating (PD) and proton-accepting (PA) molecular moieties in the S_1 state which leads to a conical intersection (CI) with the ground state.^[23] If, however, PD and PA moieties are not electronically conjugated to each other or belong to different molecular systems, the ESIPT process, or more precisely, the proton-coupled electron-transfer (PCET) process, results in the formation of a biradical pair and may lead directly to a CI (S_1/S_0) even for a coplanar orientation of molecular sub-systems.^[24,25]

In the majority of ET-relevant molecular systems, absorption of a photon promotes the system to the first excited singlet state (S_1), the so-called locally-excited (LE) state, with a polarization similar to or somewhat larger than that of the ground state (S_0). The photoinduced electron (or charge) transfer, and associated conformational changes, result in the formation of a polarized species. The ET reaction can thus be qualitatively described in terms of the Marcus-parabola of free energy. Interaction of this molecular system with a polar environment (solvent) may result in the famous inverted-parabola behavior of the ET rate constant on modulation of the free energy.^[6]

There is a growing family of polarized molecular systems where optical excitation to the ¹LE state can significantly increase the dipole moment of the system.^[26-29] Among these, a class of highly polarized molecular dyads composed of two coumarin moieties linked in a (donor-acceptor)-linker-(donor-acceptor) (DA-

FULL PAPER

L-DA) orientation, recently studied by us,^[30,31] is particularly interesting. However, flexibility of the amide linker used in these studies results in very complex photophysical behavior, related to both thermo- and photo-chemical populations of numerous conformers. This observation prompted us to study the photophysics of such systems at a more fundamental level. In this respect, we designed two strongly polarized coumarin derivatives possessing a CONH linker in position 3 to an aryl substituent of differing electronic character i.e. one possessing an electron-donating and one an electron-withdrawing substituent. The final choice of substituents was governed by the desire to achieve excellent solubility in a broad range of solvents, which was critical for studies of solvatofluorochromism.



(a) H-Amide-Ph

(b) Amide-PhF₅

(c) Ester-Ph

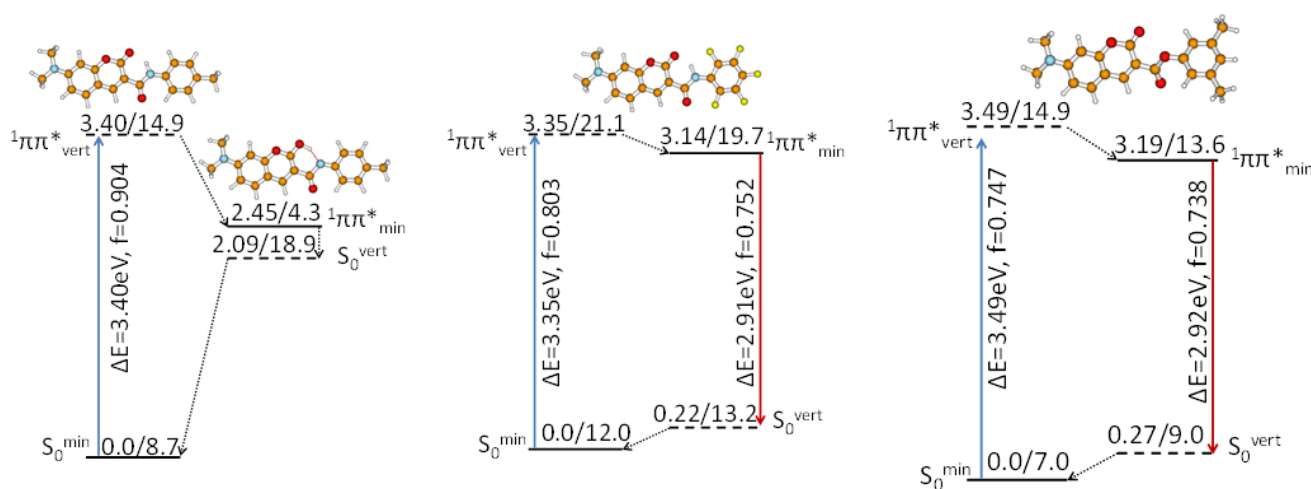


Figure 1. Vertical absorption (blue arrows) and fluorescence (red arrows) transitions, and radiationless relaxation (dashed arrows) of investigated systems computed at the ADC(2)/cc-pVDZ level of theory. Numbers denote the energy (in eV) and dipole moment (in Debye) computed for a given state. Solid lines denote adiabatic (optimized) energy of a given state while dashed lines denote 'vertical' energy of the relevant state computed at that geometry.

Absorption spectra of the investigated systems are dominated by the fully allowed ($f = 0.8-0.9$) transition to the first excited singlet state of the $\pi\pi^*$ electronic transition located vertically around 3.4 eV at this theoretical level. Geometry optimization of the S_1 state resulted in stable *trans* structures in the case of **Ester-Ph** and **Amide-PhF₅** which are predicted to fluoresce at about 2.9 eV (Figure 1b and Figure 1c). Excited-state geometry optimization of the **H-Amide-Ph** system, however, resulted in a spontaneous excited-state intramolecular proton transfer (ESIPT) process from the amide moiety to the carbonyl group of coumarin (Figure 1a). As a result, the S_1 - S_0 energy gap is reduced to 0.36 eV which precludes observation of any emission. Instead, internal conversion to the ground state is

Scheme 1. Coumarins investigated in this study.

These molecules are denoted as **Amide-PhF₅**, **H-Amide-Ph** and **D-Amide-Ph** in Scheme 1. The fourth molecule **Ester-Ph** was designed as a model lacking the ability to form an intramolecular hydrogen bond. These compounds were synthesized using standard coupling reagents from 7-(diethylamino)-2-oxo-2H-chromene-3-carboxylic acid and the corresponding amines and phenols.

Results and Discussion

Theoretical explorations

For all three investigated compounds the most stable structure on the potential-energy (PE) surface of the ground state has the *trans* conformation of the inter-ring amide or ester linker (c.f. inserts in Figure 1). In these theoretically explored systems, the terminal aliphatic groups were replaced by methyl groups. This only has a marginal influence on the electronic properties of the systems but significantly speeds up excited-state explorations at the *ab initio* theoretical level.

predicted to be the dominant deactivation channel of optical excitation of this system. All investigated systems are highly polarized in the ground state ($\mu_0 = 7-12$ D, Figure 1), and electronic excitation to the lowest $1\pi\pi^*$ state increases their polarization significantly ($\mu_1 = 15-21$ D, Figure 1), but the ESIPT process reduces the dipole moment of the **H-Amide-Ph** system to 4.3 D in the S_1 state (Figure 1a).

The radiationless decay channel associated with the ESIPT process is not present in **Ester-Ph** because of the lack of a 'mobile' hydrogen-bonded proton. Interestingly, ESIPT does not occur spontaneously in **Amide-PhF₅** which contains such a proton. The electron withdrawing nature of the -PhF₅ moiety apparently acts as a barrier for this reaction. To investigate this

FULL PAPER

idea in more detail, calculations of the potential-energy (PE) profiles along the PT reaction coordinate (NH distance) were performed and the results are presented in Figure 2b. PE profiles were optimized in the excited singlet state (S_1) and the 'vertical' energy of the ground state was computed along such determined minimum-energy reaction paths.

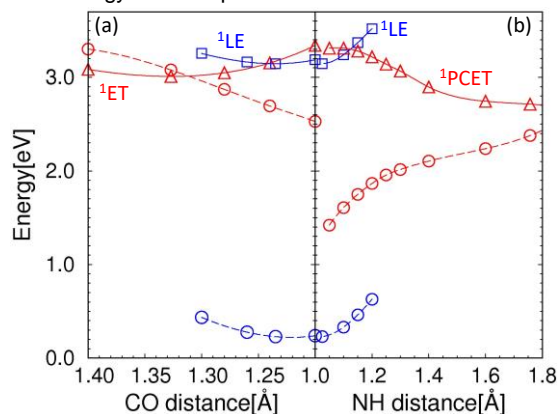


Figure 2. Potential-energy (PE) profiles of **Amide-PhF₅** computed in the S_1 state (symbols connected by solid lines) along the minimum-energy path (MEP) for electron transfer (ET, left panel) and for proton coupled electron transfer (PCET, right panel). Circles connected by dashed lines denote vertical-energy profiles of the ground state computed along the respective MEP. Squares denote the locally-excited (LE) state; triangles denote the respective charge-transfer (ET and PCET) states.

It can be noticed upon inspection of Figure 2 that the minimum-energy PE profile (MEP) of the 1LE state, which involves

a 'local' excitation within the coumarin core (Table 1a), is an increasing function of the proton-transfer reaction coordinate (NH distance, squares in Fig. 1b) and at a certain value of the NH distance (around 1.0-1.15 Å) it crosses with another MEP which is a decreasing function of the coordinate (triangles in Fig. 2b). Thus, transfer of a proton from the amide linker to the coumarin core in **Amide-PhF₅** requires elongation of the NH bond and has the energy barrier seen in Figure 2b. As a result, **Amide-PhF₅** should be fluorescent in a vacuum and solvation should result in further stabilization of the highly polarized LE state and therefore increase the barrier for a PCET process. Similarly to **H-Amide-Ph** (Figure 1a), the proton transferred form of **Amide-PhF₅** shows a very small energy gap with the ground state, and in effect the ESIPt process provides a channel for radiationless deactivation of an optical excitation. The crossing between MEP profiles of the S_1 state visible in Figure 2b is an apparent crossing since these reaction paths differ in many other intramolecular coordinates as it is reflected by different vertical PE profiles of the ground state computed along these coordinates. This also indicates that proton transfer is a non-adiabatic process induced by electron transfer between molecular moieties (Table 1b). This is a rather unexpected result for an ESIPt process which generally occurs on an adiabatic PE surface of the excited state, i.e. electron follows the proton adiabatically over the course of the reaction.^[32] A possible explanation for this effect is that the proton donating (amide-NH) and proton accepting (coumarin-C=O) moieties are not electronically conjugated to each other. In other words, a more proper classification of this reaction is the electron-driven proton transfer (EDPT)^[32] or more commonly abbreviated as proton coupled electron transfer (PCET).^[33-38]

Table 1. Nuclear conformation and electronic structure of **Amide-PhF₅** computed at the most crucial points of the S_1 PE landscape of Figure 2.

(a) 1LE state (NH = 1.1Å) $\mu_1 = 19.8$ D, $\mu_0 = 13.2$ D	(b) 1PCET state (NH = 1.1Å) $\mu_1 = 3.2$ D, $\mu_0 = 17.2$ D	(c) 1ET state (minimum) $\mu_1 = 4.9$ D, $\mu_0 = 15.3$ D
LUMO		
HOMO		

FULL PAPER

To discuss this phenomenon in more detail, the electronic structure of the LE and PCET states determined at the same value of the PT coordinate (NH = 1.1 Å) are shown in Table 1. It can be seen that for the ¹LE state (Table 1a) both the singly occupied HOMO and LUMO are localized on the coumarin moiety, but in the ¹PCET state (Table 1b) the HOMO is localized on the -PhF₅ moiety. In effect, a positive charge (hole) is transferred from the coumarin to -PhF₅ resulting in partial neutralization of the charge distribution (μ_1 : 19.8 D \rightarrow 3.2 D) which provides a driving force for the PT reaction which leads to further reduction of μ_1 to 1.82 D at the minimum of the ¹PCET state (Table ST12b of the ESI). The S₁-S₀ energy gap is only 0.34 eV at the minimum of the ¹PCET state (NH = 1.75 Å), and the system relaxes to the ground state via internal conversion.

The last stable point along the proton transferring MEP was obtained upon shrinking the NH distance to 1.05 Å. An unconstrained geometry optimization starting from this point resulted in another solution, which is illustrated in Figure 2a and in Table 1c. In this geometry (C=O bond length around 1.33 Å) the ground state (red circles in Figure 2a) is located slightly (0.07 eV) above the S₁ state. This means a conical intersection between the states is located near to this geometry. By inspecting the electronic structure of the S₁ state at its equilibrium geometry (Table 1c) the same molecular orbitals as in the ¹PCET state (Table 1b) are involved, and the state has a pure electron-transfer (ET) character, however, the nuclear geometries of these states are essentially different. In the ¹PCET state at NH = 1.1 Å a strong hydrogen bond R(O...H) = 1.35 Å which facilitates the PT process is formed. On the contrary, in the ¹ET state the hydrogen bond is broken (R(O...H) = 2.37 Å) and the amide moiety is strongly twisted and pyramidized. However, a close inspection of the equilibrium geometry of the ¹ET state shows many intramolecular coordinates are involved in the reaction. The most remarkable is the perpendicular orientation of the coumarin core and the benzene rings in the ¹ET state vs. 53° at the ¹LE equilibrium. Thus formally, this state can be classified as a TICT state. There is also a significant elongation of the coumarin C=O bond length from 1.24 Å in the ¹LE state to 1.33 Å in the ¹ET state (Table 1). The latter was chosen as the reaction coordinate for optimization of the ET reaction pathway. PE profiles computed along this reaction coordinate are shown in Figure 2a.

Inspection of the PE profiles of Figure 2a shows that the ¹LE state is crossed by the ¹ET state close to the bottom of the former state. Once again, this is only an apparent crossing since many other intramolecular coordinates are involved in the reaction, and relaxation along these coordinates results in a large shift of the PE profile of the ground state along this reaction path. On the other hand, the ¹TICT/S₀ crossing, visible in Figure 2a as red circles/red triangles lines crossing, is a real crossing since both PE profiles are computed along the same reaction path. Thus, a non-adiabatic transition from the locally-excited S₁ fluorescing (¹LE) state to the charge-transfer state, accompanied by either transfer of the proton (¹PCET state) or by structural relaxation along other intramolecular coordinates (¹TICT state), is deleterious for fluorescence due to internal conversion to the ground state.

In summary, both TICT and PCET processes provide a source of radiationless deactivation of an optical excitation and compete with fluorescence as relaxation pathways for the system. Since these states are of a different electronic nature than the fluorescing ¹LE state and different intramolecular coordinates are

involved for these processes, complex photophysical behavior depending on both chemical substitutions and on environment is expected to be observed for this system. A particularly interesting and intriguing aspect of the observed photophysical phenomenon is related to the fact that the ¹LE state is highly polarized (μ_1 = 15-20 D, Figure 1), and the competing TICT and PCET processes result in formation of relatively non-polarized states. This is rather exceptional for ET process, since an increase in solvent polarity is expected to destabilize ¹TICT (and ¹PCET) states with respect to the polarized S₀ and ¹LE states which may result in an increase of the barrier for these processes and in effect may increase the fluorescence yield vs. polarity of the solvent.

Experimental investigations

Existence of an intramolecular hydrogen bond in **H-Amide-Ph** and **Amide-PhF₅** was investigated in both the solid state and in solution. Crystals of compounds **H-Amide-Ph** and **Amide-PhF₅** suitable for X-ray crystallography were obtained by slow diffusion of hexane into a solution of the appropriate compound in dichloromethane. X-ray analysis clearly proved the existence of a hydrogen bonding interaction between the amide proton and carbonyl oxygen of the coumarin moiety (Figure SF3 of the ESI). The hydrogen bond length for **Amide-PhF₅** and **H-Amide-Ph** is 1.905 Å and 2.003 Å, respectively. The dihedral angle between coumarin core and arylamide substituent for **H-Amide-Ph** is 23.84° while **Amide-PhF₅** is more twisted and the angle is 45.76°. This difference is probably related to the fact that the intramolecular hydrogen bond in **Amide-PhF₅** is weaker than in **H-Amide-Ph** and hence the aniline moiety is more twisted with respect to the coumarin core. The packing diagrams of **Amide-PhF₅** and **H-Amide-Ph** indicate that the molecules are arranged in head-to-tail manner (Figure SF4 of the ESI).

It is well known that the chemical shift of a proton is proportional to the strength of a hydrogen bond it is involved in,^[39,40] so NMR can be used as a technique for the characterization of hydrogen bonding in solution. To investigate the influence of solvents on hydrogen bonds in **Amide-PhF₅** and **H-Amide-Ph**, we performed additional NMR measurements in selected polar and non-polar solvents (Figure SF5). The chemical shifts for both molecules behave similarly: in non-polar benzene or solvents of low polarity (chloroform), the signals from the amide protons are more upfield shifted, while in polar dimethyl sulfoxide the signals remain in a downfield position. This reveals that the intramolecular hydrogen bond is strong in non-polar solvents but weakens in polar ones. The bond is stronger in **H-Amide-Ph** than in **Amide-PhF₅** as chemical shifts for the former are larger than for the latter (Figure S5b, lines from 10.5 to 11.25 and S5a, lines around 10.5 respectively). The electron withdrawing -PhF₅ group reduces the electron density on the NH hydrogen and leads to the weaker H-bonding. This is consistent with the observation that the energy of the NH vibration in **H-Amide-Ph**, 3262 cm⁻¹, is slightly higher than in **Amide-PhF₅**, 3245 cm⁻¹, proving the larger strength in the former molecule (Figure S6).

The shape of the optical spectra of the three molecules in *n*-hexane are similar and are positioned at comparable energies (Figure 3). Small differences between the maxima of the absorption spectra in *n*-hexane (24155, 24213 and 24570 cm⁻¹ for **Amide-PhF₅**, **H-Amide-Ph** and **Ester-Ph**, respectively), reveal that the hydrogen bond present in **Amide-PhF₅** and **H-Amide-Ph** lowers the energy of the S₁ state.

FULL PAPER

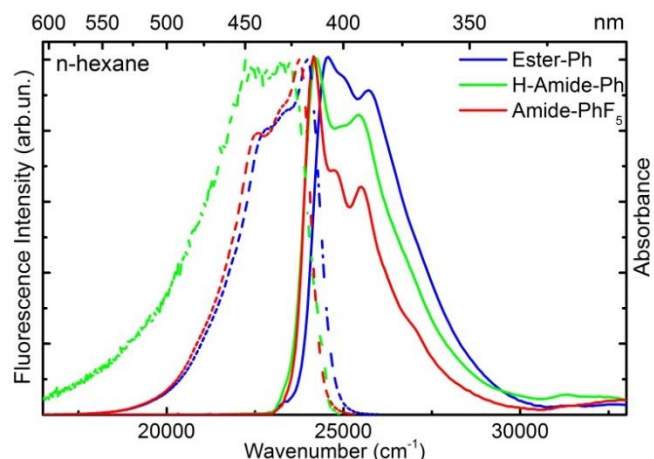


Figure 3. Absorption (solid lines) and normalized fluorescence spectra (dashed lines) of **Amide-PhF₅**, **H-Amide-Ph** and **Ester-Ph** in *n*-hexane recorded with excitation at 390 nm. Legend specifies colours of lines.

The absorption spectra only shift slightly with regard to solvent polarity. In contrast, the fluorescence spectra show much more pronounced solvatochromism (Figure SF7, SF11 and SF15 of the ESI), which points to a substantial increase of the electric dipole moment in the excited state (μ_e) in comparison to its value in the ground state (μ_g). From the slopes of the solvatochromic dependencies of absorption spectra the energy of the first excited state in the gas phase may be determined (see section 5.1 of ESI for the method used and ESI sections 5.3 to 5.5 for data elaboration). The experimental values (24160 cm^{-1} or 3.0 eV, 24290 cm^{-1} or 3.01 eV and 24613 cm^{-1} or 3.05 eV for **Amide-PhF₅**, **H-Amide-Ph** and **Ester-Ph**, respectively) can be compared with those obtained through calculations (3.35 eV, 3.4 eV and 3.49 eV).

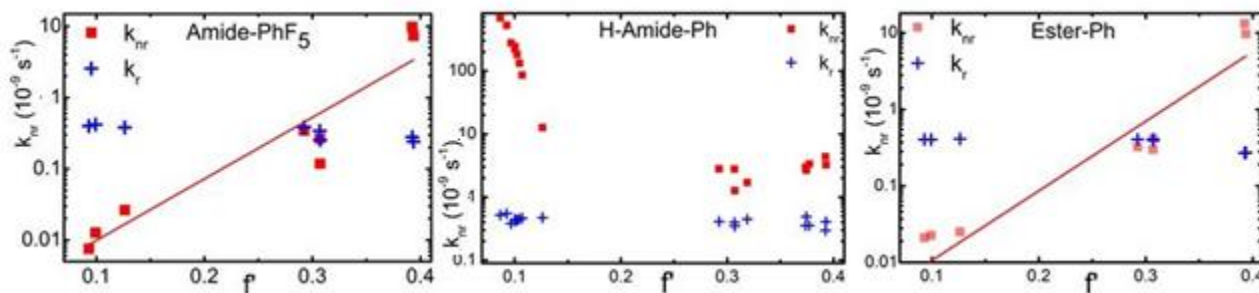


Figure 4. Semilogarithmic plot of radiative (k_r , blue crosses) and non-radiative (k_{nr} , red squares) deexcitation rates of **Amide-PhF₅** (left), **H-Amide-Ph** (middle) and **Ester-Ph** (right) versus modified Lippert-Mataga parameter $f = [(\epsilon - 1)/(2\epsilon + 1) - 0.5 \times (n^2 - 1)/(2n^2 + 1)]$ in solvents. Solid lines represent linear fits to k_{nr} data.

The growth of k_{nr} observed for the **Amide-PhF₅** and **Ester-Ph** in polar solvents (Figure 1) is assigned to an increase in the internal conversion rate induced by nuclear rearrangement related to electron transfer which leads to a conical intersection with the ground state (see sections 5.3 to 5.6 of the ESI). Similar phenomenon have previously been observed for other 7-aminocoumarin derivatives and assigned to stabilization of a dark TICT state.⁵⁰ Indeed, in the solid state, where large amplitude motions are hindered, fluorescence decays of all molecules studied are hundreds of nanoseconds long (Figure SF20).

Amide-PhF₅, a compound lacking proton transfer, may be treated as a model molecule for **H-Amide-Ph** in evaluation of the PCET rate constant. PCET rates for **H-Amide-Ph**, k_{PCET}^H , and **D-**

The experimental energy values differ from the calculated ones by ca. 0.3–0.4 eV, a typical overestimation of excitation energy at this theoretical level.^[41] The excited-state increase of dipole moment calculated from solvatochromic slopes and expressed as the μ_e/μ_g ratio (3.53, 2.8 and 2.9 - for **Amide-PhF₅**, **H-Amide-Ph** and **Ester-Ph** respectively; see ESI sections 4.3 to 4.5 for details) as well as the calculated values (1.76, 1.7 and 2.05) point to a large increase of μ upon photoexcitation. This corroborates the fact that the three molecules studied are push-pull compounds, with a remarkable charge shift due to an optical transition.

The influence of solvent on the fluorescence quantum yield Φ_F and decay time τ_F depends strongly on the molecule. **Amide-PhF₅** and **Ester-Ph** have very high Φ_F exceeding 0.9 and long $\tau_F \approx 2.4$ ns in several non-polar solvents (Tables ST4 and ST6 of the ESI). In polar solvents, Φ_F drops to 0.02 and τ_F shortens to below 100 ps. Very different and complex behaviour is observed for **H-Amide-Ph**: in *n*-hexane it has very weak emission with low $\Phi_F = 0.001$ and short $\tau_F \approx 2$ ps. In longer *n*-alkanes, toluene and solvents of low dielectric constant ($\epsilon < 10$) both parameters increase to reach maximal values in dichloromethane and 1,2-dichlorobenzene ($\Phi_F = 0.22$ and $\tau_F = 620$ ps, Table ST5). In more polar solvents ($\epsilon > 10$) the fluorescence quantum yield decreases to 0.063 and decay time to 214 ps. Fluorescence decays are single exponential for all molecules (Figure SF8, SF13 and SF17), so one may estimate the radiative k_r and non-radiative k_{nr} rate constants from the formulas: $k_r = \Phi_F/\tau_F$ and $k_{nr} = 1/\tau_F - k_r$. In the three molecules studied the radiative rate constant is nearly constant in all solvents, while the non-radiative rate constant for **Amide-PhF₅** and **Ester-Ph** grows with solvent polarity, in **H-Amide-Ph** it has a more complex behaviour – strongly decreasing with the solvent polarity parameter f in non-polar and polarizable solvents and slightly growing with polarity in polar solvents (Figure 4 and Tables ST4 to ST6).

Amide-Ph, k_{PCET}^D , can be calculated as a difference between non-radiative rates of these molecules, k_{nr}^{H-Ph} and k_{nr}^{D-Ph} respectively, and the rate of **Amide-PhF₅**, $k_{nr}^{PhF_5}$, i.e. $k_{PCET}^H = k_{nr}^{H-Ph} - k_{nr}^{PhF_5}$, and $k_{PCET}^D = k_{nr}^{D-Ph} - k_{nr}^{PhF_5}$. So obtained PCET rates are presented in Figure 5, as semilogarithmic plot of PCET rate constants depicted versus energy of the fluorescent LE state, the initial state for the transfer process. A linear decrease of the PCET rate constant is observed over a wide range of solvents (*n*-alkanes, toluene, ethyl acetate, tetrahydrofuran and dichloromethane) where PCET rate constants are higher than that of the competing radiationless decay channel caused by benzene ring twist. This result indicates that the barrier for the PCET process is modulated by solvation of the S_1 (LE) state. Both theory

FULL PAPER

and solvatochromism of absorption and fluorescence spectra (Figure SF11) set the 0-0 transition for the LE state in the gas phase at 3.0 eV. Using the linear fit parameters of Figure 5 for this energy, a gas phase PCET rate constant of $5.64 \times 10^{12} \text{ s}^{-1}$ can be obtained.

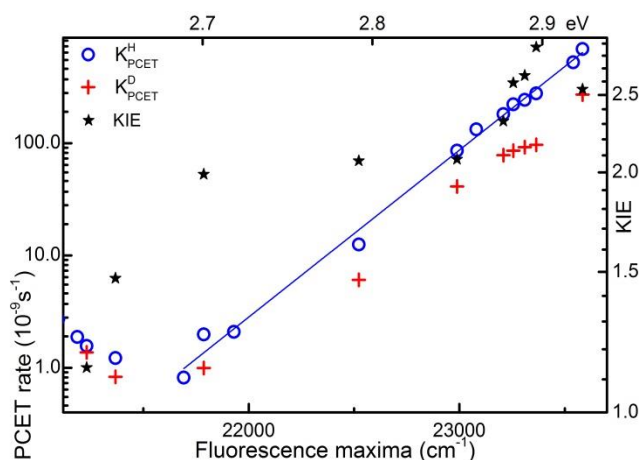


Figure 5. Semilogarithmic plot of PCET rates of **H-Amide-Ph**, ($k_{\text{PCET}}^{\text{H}}$, blue circles), **D-Amide-Ph**, ($k_{\text{PCET}}^{\text{D}}$, red crosses) left vertical axis, and kinetic isotope effect rate ($\text{KIE} = k_{\text{PCET}}^{\text{H}}/k_{\text{PCET}}^{\text{D}}$, black stars) versus the energy of fluorescence spectra maxima.

Discussion

For **H-Amide-Ph** in the gas phase, theory predicts a fast, barrierless, nonadiabatic PCET (Figure 6 and 1a). Weak fluorescence of **H-Amide-Ph** in *n*-pentane reveals that a small barrier already exists in this inert solvent. This intuitively may be understood, as the solvent increases the reorganization energy, λ , and decreases the driving force, ΔG . Indeed, in **H-Amide-Ph** the initial state for PCET process, the LE state, has much higher dipole moment, $\mu_{\text{e}} = 15 \text{ D}$, than the final CT state, $\mu_{\text{CT}} = 4.3 \text{ D}$, so the LE state should be more stabilised by the solvent than located at a lower energy CT state, so as a result ΔG should decrease with dielectric solvation. As a consequence of the solvent-induced change of both factors, increasing λ and decreasing ΔG , the molecular system is detuned from the optimal ET condition of $\lambda \approx -\Delta G$, which slows down the transfer rate in the normal Marcus region.

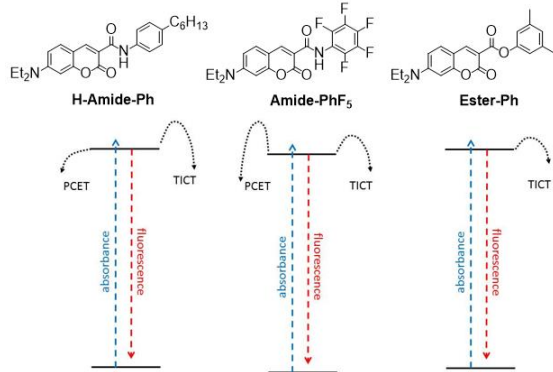


Figure 6. Simplified diagram of the photophysical processes that compete with each other for the deactivation of optically populated ^1LE state in the molecules studied: **H-Amide-Ph** (left), **Amide-PhF₅** (middle), and **Ester-Ph** (right). For transparency only the ground (lower) and ^1LE (upper) states are shown.

Transitions are sketched out by arrows: optical - absorption and emission (dashed lines), radiationless - PCET and ET (dotted lines).

This phenomenon occurs because the initial LE state has a much higher dipole moment than the final CT state. The fluorescent LE state enables monitoring of its solvation and PCET rate constant in a wide range of solvents, which gives an interesting perspective on the transfer mechanism and factors influenced by solvent.

Kinetic isotope effect decreases at high energy barrier

The theory for the PCET process was developed as an extension of the Marcus electron transfer model by Cukier and Nocera^[51] and by Hammes-Schiffer and Soudackov.^[52] In the general PCET theory the transferring proton and the active electrons are treated quantum mechanically, and the PCET reaction is described in terms of nonadiabatic transitions between mixed electron-proton vibronic states. The rate constant of the PCET process between the initial μ and final ν vibronic states is expressed as:^[53]

$$k_{\text{PCET}}(R) = \sum_{\mu, \nu} \frac{P_{\mu}}{h} |V^{\text{el}} S_{\mu\nu}|^2 \sqrt{\frac{\pi}{\lambda k_{\text{B}} T}} \exp\left(-\frac{(\Delta G_{\mu\nu}^0 + \lambda)^2}{4\lambda k_{\text{B}} T}\right) \quad (1)$$

where P_{μ} is the Boltzmann population reactant state, V^{el} is the electronic coupling, $S_{\mu\nu}$ is the overlap integral between the proton vibrational wave function of reactant and product states that depends on the proton donor-acceptor distance R , $\Delta G_{\mu\nu}^0$ is the reaction free energy associated with vibronic state pair (μ , ν) and λ is the total reorganization energy. T and k_{B} denote the absolute temperature and Boltzmann constant, respectively. The overall PCET rate constant is obtained by thermal averaging of the rate expressed in eq. 1 weighted by the probability of sampling a given proton donor-acceptor distance R : $k_{\text{PCET}} = \int k_{\text{PCET}}(R) P(R) dR$.^[53] The theory has been successfully applied to PCET processes in the Marcus normal as well as in inverted regions,^[53] and to describe the kinetic isotope effect (KIE).^[54] The theory reveals the effect of the contribution to the rate constant is not only from the ground vibronic state (0,0 pair) but also from excited vibronic states due to larger overlap integrals of excited states.^[53] This decreases KIE because the excited vibronic states are associated with larger overlaps and therefore a smaller ratio of hydrogen to deuterium overlaps.^[54] The effect is observed for **H-Amide-Ph** and **D-Amide-Ph** in polar solvents, where the barrier increases and PCET reaction slows down (Figure 5).

PCET rate constant correlates with solvatochromism of fluorescence spectrum

The PCET process in **H-Amide-Ph** occurs between the initial higher and very polarized $S_1(\text{LE})$ state and the final lower and much less polarized CT state. Fluorescence from the $S_1(\text{LE})$ state to the less polarized S_0 state is also connected with a remarkable change of charge distribution. Thus, a substantial charge shift occurs in both transitions. The analogy between an optical CT transition (radiative relaxation process) and electron transfer process has been shown already by Marcus.^[42] For a single high-frequency intramolecular vibration ($h\nu > 1000 \text{ cm}^{-1}$) a formula for the fluorescence spectrum of bridged DA molecules was derived^[43]

FULL PAPER

$$I(\nu) = e^{-S} \sum_{n=0}^{\infty} \frac{S^n}{n!} \exp\left(-\frac{(\Delta G + h\nu + nh\nu_i + \lambda_s)^2}{4\lambda_s k_B T}\right) \quad (2)$$

where ΔG is the free energy change, h is the Planck constant, ν is frequency of light, ν_i is the frequency of high frequency intramolecular vibration, λ_s is the solvent reorganization energy, and $S = \lambda_i/h\nu_i$, λ_i is the intramolecular reorganization energy. Following the above mentioned analogy, the rate constants for radiative charge recombination in DA molecules,^[44] as well as for non-radiative electron transfer^[45] were also proposed. This allowed for the formulation of the charge recombination rate k_{nr} in the form^[46]

$$k_{nr} = \frac{4\pi}{h} V_{AD}^2 \sum_{n=1}^{\infty} \frac{e^{-S} S^n}{n!} \frac{1}{\sqrt{4\pi\lambda_s k_B T}} \exp\left(-\frac{(\Delta G + nh\nu_i + \lambda_s)^2}{4\lambda_s k_B T}\right) \quad (3)$$

where V_{AD} is the electronic coupling element between the two states involved in the transition. The fluorescence spectrum of **H-Amide-Ph** in *n*-alkanes and toluene is dominated by the vibronic progression at 1150 cm⁻¹ (Figure SF12 and section 5.4 of ESI), justifying usage of eq. 2. This feature and the similarity between expressions (1), (2) and (3) suggested that k_{PCET} values could be plotted against the position of fluorescence spectrum maximum $h\nu_{fl}^{max}$. The good (*R*-Square = 0.9945) linear dependence of k_{PCET} on $h\nu_{fl}^{max}$ observed in Figure 5 for several solvents from *n*-pentane to dichloromethane confirms the relationship between the two observables and justifies the approach. Indeed, k_{nr} in Figure 4b and $h\nu_{fl}^{max}$ presented in inset to Figure SF11a behave in the same way with solvent polarity parameter *f* - they decrease abruptly in non-polar solvents and much slower in polar ones.

Electron transfer triggers proton transfer or TICT depending on energy barrier

Both non-radiative processes occurring in **H-Amide-Ph** are associated with electron transfer. This is clear when one compares the HOMO and LUMO orbitals involved in the LE state (Table ST8 in analogy with Table 1a) with the relevant orbitals of the TICT and PCET states where the electron density localized on the coumarin rings of the former state moves to the benzene ring in the latter states (Tables ST11a and ST11b). Optical excitation shifts the charge from the electron donating moiety (diethylamine) to the electron accepting coumarin, resulting in an increase of the molecular dipole moment from 9 D in the S_0 state to about 15 D in the ¹LE state (Table ST8). In the course of the TICT and PCET processes, the electronic charge shifts in the opposite direction partially neutralizing the polarization of the system, so the final states have a particularly small dipole moment of about 4-5 D (Tables ST11a and ST11b). Hence, one may consider both radiationless transitions as electron transfer processes. An electron transfer from the benzene to coumarin moiety triggers either proton transfer from NH of the amide linker onto the carbonyl oxygen (PCET) or results in elongation of the C=O double bond and inter-ring twisting that stabilizes the TICT state. Both processes lead the system to a CI with the ground state which opens internal conversion channels. The ET triggered twist occurs in polar solvents in all three dyeds. In acetonitrile the process is the fastest in **Ester-Ph** which does not have an intramolecular hydrogen bond ($\tau_F = 100$ ps) and slower in **H-Amide-Ph** ($\tau_F = 274$ ps) and **D-Amide-Ph** ($\tau_F = 288$ ps) where the hydrogen bonds are stronger.

Factors influencing electron transfer

The free energy for the ET process can be calculated using the Weller approximation for electron transfer^[55]

$$\Delta G^0 = E^0(A^+A) - E^0(DD^-) - E_{0-0} - \frac{e^2}{4\pi\epsilon_0\epsilon R_{AD}} \quad (4)$$

where $E^0(A^+A)$ and $E^0(DD^-)$ are reduction potentials of acceptor and donor parts of the dyad respectively, R_{AD} is the distance of ET and E_{0-0} approximates the free energy of difference of the initial and final state, usually LE and ground state (GS), which then can be assigned to the interception of absorption and emission spectra. In our dyad the final state is the optically dark CT state so this parameter cannot be directly observed. Electrochemical potentials depend on solvent and for single electron oxidation or reduction their values in solvents *i* and *j* of static dielectric constant ϵ_i and ϵ_j are related by the simplified formula^[13]

$$E_i = E_j + \frac{e^2}{8\pi\epsilon_0 F R} \left(\frac{1}{\epsilon_i} - \frac{1}{\epsilon_j}\right) \quad (5)$$

where *F* is the Faraday constant and *R* is the Born effective radius.

The reorganization energy, λ , is the sum of inner-sphere (solute) λ_i and outer-sphere (solvent) λ_s , reorganization energies, i.e. $\lambda = \lambda_i + \lambda_s$, for which the Marcus two-sphere model is given by

$$\lambda_s = \frac{e^2}{8\pi\epsilon_0} \left(\frac{1}{n^2} - \frac{1}{\epsilon}\right) \left(\frac{1}{R_A} + \frac{1}{R_D} - \frac{2}{R_{AD}}\right) \quad (6)$$

where R_A and R_D are the Born radius of acceptor and donor spheres respectively and R_{AD} is distance between the centers of them. The expression was derived with assumption of separated spheres, i.e. $R_A + R_D < R_{AD}$, but has also been applied for spheres in contact as demonstrated for dyads of anthracene.^[53] Let us notice, that the reciprocal of dielectric constant, the $1/\epsilon$ factor, is present in all equations (4) – (6), its value and change in non-polar or medium polarity solvents is expected to be much more than in polar solvents.

An alternative approach for the calculation of barriers and solvent reorganization energy in optical and thermal ET processes was proposed for a point dipole molecule in an Onsager cavity using the thermodynamic approach proposed by Marcus.^[56] Two “Brunschwig” solvent polarity parameters F_1 and F_2 were derived (equations SE4 and SE5 in section 5.7 of ESI) for use in expressions of ΔG change in solvent versus gas phase $\Delta G^0(\epsilon) - \Delta G^0(\epsilon = 1)$ (eq SE7) and solvent reorganization energy λ_s (eq SE6). Expressions for solvatochromism of absorption, $\Delta E_{abs}(\epsilon)$, and emission, $\Delta E_{em}(\epsilon)$, were also derived.⁵⁶ These formulas are similar to those of the reaction field method by Onsager or Lippert, but are obtained with a general method and less restrictive assumptions.

In both approaches, the total solvent relaxation energy may be related to Stokes shift, $\lambda = (\nu_{abs}^{max} - \nu_{flu}^{max})/2$, and the free energy to the mean of optical transition energy, $\Delta G = (\nu_{abs}^{max} + \nu_{flu}^{max})/2$.^[46,56] In **H-Amide-Ph** the trend from solvatochromism of spectra can be relevant to changes in ΔG for PCET as both processes originate from the highly polar ¹LE state and end up in much less polarized states. Figure SF25 of the ESI depicts Stokes

FULL PAPER

shift versus four different solvent polarity parameters. A linear trend is observed only for the reciprocal of dielectric constant (Figure SE25b). This points to the outer sphere dielectric polarisation and Born cavity model rather than a point-dipole in Onsager cavity approximation, (eq. SE1 and SE6). This is not surprising as the $1/\epsilon$ factor is present in all 4-6 equations. The 0-0 transition to the ^1LE state, important for ΔG evaluation, shows different trends in non-polar and polar solvents (Figure SE24). The $1/\epsilon$ factor offers a monotonic trend, though the Brunshwig F_1 - F_2 parameter cannot be excluded. The changes in λ and ΔG , even in non-polar solvents are clear, and both parameters lead to a lowering in energy of the ^1LE state and increase of the barrier for the PCET reaction. The parameter $(1/n^2 - 1/\epsilon)$ used for outer sphere reorganization energy λ_s leads to steep change of the PCET rate constant, Stokes shift and E_{0-0} values in n -alkanes and toluene (Figures SE23-25). The same is true for the amended Marcus formula for λ_s (eq. 7)^[57]

$$\lambda_s = \frac{e^2}{8\pi\epsilon_0} \left(\frac{1}{R_A} + \frac{1}{R_D} - \frac{2}{R_{AD}} \right) \left(\frac{1}{n^2} - \frac{1}{\epsilon} \right)^2 \frac{1}{1-\epsilon^{-1}} \quad (7)$$

which was derived to reduce overestimation of solvent relaxation energy obtained with equation (6). It is important to notice that in n -alkanes $\epsilon_{\text{static}} \approx \epsilon_{\text{optical}} = n^2$, which leads to a very steep change in quantities presented by the function of the $(n^2 - \epsilon^{-1})$ parameter. The inclusion of optical frequency dielectric constant may account for buildup of the barrier for ET already in n -alkanes, slowing down the process in addition to the substantial solvatochromism in non-polar solvents. However, inspection of figures SF23-SF25 reveals that the best correlation is observed between the Stokes shift and the $1/\epsilon$ parameter. This suggests that the slowing down of PCET process and the solvatochromism of fluorescence may originate from screening of electrostatic force in dielectric media.

Dielectric friction is another physical factor that may have an impact on the fast PCET rate.^[58] In n -alkanes at 20 °C the dielectric relaxation time, τ_D , changes from 2.4 ps in n -hexane through 2.7 ps in n -nonane to 3.2 ps in n -decane and is related to rotation of the ends of the alkyl chains because rotation of whole molecules is an order of magnitude slower.^[59] The longitudinal relaxation time, $\tau_L = \tau_D(\epsilon_{\text{optical}}/\epsilon_{\text{static}})$ is very similar to τ_D as in n -alkanes $\epsilon_{\text{static}} \approx \epsilon_{\text{optical}}$. Fluorescence decay times of **H-Amide-Ph** in n -alkanes related to the PCET process, increase faster with chain length than τ_L values, and decay times of **D-Amide-Ph** are longer than the longitudinal dielectric relaxation times (Table ST7), which indicates dielectric friction is not the main factor limiting the PCET rate. The next factor influencing the PCET process is the strength of $\text{NH}\cdots\text{O}$ hydrogen bond which decreases with solvent polarity as revealed in Figure SF5. A weaker HB requires larger distances being penetrated for PCET to occur. This translates to a higher barrier for the process. Solvent polarity affects the barrier in the same direction through stabilisation of the ^1LE state, so disentanglement of the two factors influence remains a challenge. Hydrogen bonding with protic solvent molecule provides another channel competing with PCET and reducing its rate. The external H-bond and other solvent – specific interactions, changing photophysics of a molecule, were not a subject of this study.

Mechanistic aspects of electron transfer

The above considerations provide, however, only a phenomenological explanation of experimental observations, discussed in an analogy to the Marcus theory of electron transfer.^[47] Since excited-state analytical gradients are not so far available for dielectric solvation models, in order to provide more insight into the mechanistic aspects of the observed phenomena we performed excited-state geometry optimization of the **H-Amide-Ph** molecular system as a complex with a single molecule of the polar solvents acetonitrile and methanol. The results of this are presented in Tables ST13a and ST13b of the ESI, respectively. It can be noticed upon inspection of the Table ST13a that the interaction of **H-Amide-Ph** with a single acetonitrile molecule hinders the PCET reaction by stabilization of the LE state. A similar effect is also observed for the complex with a methanol molecule (Table 13b). Additionally, the protic methanol molecule competes with the intramolecular hydrogen bond. This hinders the PCET process to a greater extent, but on the other hand promotes the ET process by twisting the benzene ring with respect to the coumarin core. Both polarized solvent molecules reduce the S_1/S_0 energy gap, an effect which is stronger for the complex with methanol, supporting the larger bathochromic shift of fluorescence in this solvent and the increase of internal conversion to the ground state. These effects are in full accord with experimental results and provide a mechanistic explanation of our observations.

Other non-radiative processes

For unsubstituted coumarin and 7-hydroxycoumarin two other non-radiative mechanisms have been reported: breaking of the lactone bond leading to ring opening and transition into a dark $n\pi^*$ state along the carbonyl stretching mode.^[48] Both mechanisms were proposed for the ultrafast radiationless relaxation observed in unsubstituted coumarin, where electron density on the lactone ring is low.^[48,49] The non-radiative processes in coumarin derivatives studied in this work are slower and do not lead to any photochemical products. Theoretical calculations do not predict ring cleavage for **H-Amide-Ph**, **Amide-PhF₅** or **Ester-Ph**. In light of both these results and in obvious relation to the fast radiationless relaxation with the existence of a $\text{NH} - \text{carbonyl oxygen hydrogen bond}$ we excluded ring opening from interpretation of our experimental results. Therefore, we conclude that the radiationless relaxation observed in the investigated coumarin derivatives is a manifestation of the occurrence of two competing processes: PCET and TICT, which through CI with the ground state, lead to efficient internal conversion.

Conclusions

In conclusion, the slight structural modification of classical push-pull coumarins possessing electron-donating groups at position 7 and electron-accepting groups at position 3 leads to significant changes in their photophysics through lowering of the CT energy state. Replacing a $-\text{CO}_2\text{Et}$ moiety with a secondary aromatic amide triggers proton-coupled electron transfer (PCET) and twisted intramolecular charge transfer (TICT) processes. Excited-state properties are strongly dependent on the electron-withdrawing character of the aryl substituents located on the nitrogen atom. If a $-\text{CONHPhF}_5$ group is present, a high barrier for

FULL PAPER

PCET occurs in all solvents resulting in strong fluorescence and long lifetimes in non-polar and moderately-polar solvents. Replacing -PhF₅ with the electron-donating -C₆H₄C₆H₁₃ causes PCET to be the dominant process in non-polar solvents, while in polarizable toluene and in polar solvents, the observed increase in Φ_F and τ_F indicate a slowdown of the PCET which points to an increase in the barrier for the process. Replacing amides with a phenol-derived ester linker removes the deexcitation channels related to PCET, and fluorescence from a locally excited-state is strong in non-polar and in weakly polar solvents.

Computational studies have revealed that the photophysics of the investigated molecular systems are determined by competition between the PCET and TICT processes. Both processes are initiated by electron transfer from the excited coumarin core to the molecular moiety substituted at position 3. If both molecular subsystems are tightly hydrogen bonded to each other, the CT state is populated and stabilized by ET triggering the PCET process. If, however, the hydrogen bond does not exist, like in **Ester-Ph**, or is weakened due to interaction with polar or protic solvent, the CT state is stabilized by a mutual twist of the electron-donating and electron-accepting moieties (TICT process). Both photophysical processes lead to conical intersections with the ground state and provide channels for radiationless decay that compete with fluorescence. In all cases, since dipole moments of charge-separated TICT and PCET states formed in the photoreaction are much smaller than dipole moments of the LE state they proceed through, the barrier for these processes is sensitive to interaction with the environment.

The experimentally elucidated photophysical properties, including the strong dependence of the fluorescence quantum yield on solvent polarity fully corroborate these theoretical findings. This unusual phenomenon is strongly associated with the fact that in both TICT and PCET processes, the electronic charge shifts in an opposite direction to that induced by an optical excitation partially neutralizing polarization of the system, so the final states have a particularly small dipole moment of about 4-5 D. The PCET process is controlled by the solvent through dielectric solvation of the highly polarized S₁ state, and shows a moderate kinetic isotope effect (< 3) that decreases at higher barriers in agreement with the general theory developed for proton transfer as an extension of the Marcus ET model.

Experimental Section

The description of methods and tools used in this study as well as detailed results are presented in Supporting Information (synthesis, experimental and spectroscopic methods, optical results, computational methods and theoretical results, IR and NMR spectra, crystallographic and NMR data). In particular, sections 5.3 ÷ 5.7 contain detailed presentation and discussion of optical spectroscopy results for all molecules (**H-Amide-Ph**, **D-Amide-Ph**, **Amide-PhF₅** and **Ester-Ph**) in solvents, in anhydrous solvents and in powder.

Synthesis of Amide-PhF₅. 7-(Diethylamino)-2-oxo-2H-chromene-3-carboxylic acid **1** (1.0 mmol), PyCIU (1.15 mmol) and dry DCE were placed in a dry Schlenk flask under argon. *N,N*-Diisopropylethylamine (3.45 mmol) was subsequently added and the reaction mixture was stirred for 30 min at room temperature. Then, pentafluoroaniline **2** (0.77 mmol) was added and the mixture was heated at 85 °C for 24 h under argon. Then, the mixture was cooled to room temperature, diluted with water and extracted with DCM. The combined organic layers were dried over Na₂SO₄ and concentrated under reduced pressure. The crude product was purified by

column chromatography (silica, DCM). Crystallization from DCM-hexane afforded product of analytical purity. Yield: 0.260g, 79%; m.p. 207-208 °C; ¹H NMR (500 MHz, CDCl₃, 25 °C, TMS): δ = 10.39 (s, 1H, NH), 8.77 (s, 1H, CH), 7.48 (d, *J* = 9.0 Hz, 1H, Ar), 6.72 (dd, *J* = 9.0, 2.5 Hz, 1H, Ar), 6.56 (d, *J* = 2 Hz, 1H, Ar), 3.49 (q, *J* = 7.0 Hz, 4H, NCH₂CH₃), 1.27 (t, *J* = 7.0 Hz, 6H, NCH₂CH₃); IR (KBr, cm⁻¹): 791, 1009, 1135, 1205, 1354, 1493, 1512, 1580, 1619, 1712, 2979, 3213; HRMS (ESI-TOF): *m/z* calculated for C₂₀H₁₅F₅N₂O₃[M+H]⁺ = 449.0896; found: 449.0901 (+Na); Elemental analysis (%): calculated for C₂₀H₁₅F₅N₂O₃: C, 56.34; H, 3.55; N, 6.57; found: C, 56.26; H, 3.38; N, 6.50.

Synthesis of H-Amide-Ph. To the solution of 7-(diethylamino)-2-oxo-2H-chromene-3-carboxylic acid **1** (1.0 mmol) in dry DCE, EDC (1.5 mmol), DMAP (cat. amount) and 4-*n*-hexylaniline **3** (1.0 mmol) were added and the reaction mixture was stirred at room temperature for 12 h under argon. The mixture was diluted with water and extracted with DCM. The combined organic layers were dried over Na₂SO₄ and concentrated under reduced pressure. The crude product was purified by column chromatography (silica, DCM). Crystallized from DCM-hexane afforded product of analytical purity. Yield: 0.380g, 83%; m.p. 168-169 °C; ¹H NMR (500 MHz, CDCl₃, 25 °C, TMS): δ = 10.79 (s, 1H, NH), 8.79 (s, 1H, CH), 7.63 (d, *J* = 8.0 Hz, 2H, Ar), 7.47 (d, *J* = 9.0 Hz, 1H, Ar), 7.16 (d, *J* = 8 Hz, 2H, Ar), 6.71 (dd, *J* = 8.0, 2.0 Hz, 1H, Ar), 6.57 (d, *J* = 2.0 Hz, 1H, Ar), 3.47 (q, *J* = 8.0 Hz, 4H, NCH₂CH₃), 2.58 (t, *J* = 8.0 Hz, 2H, CH₂(CH₂)₄CH₃), 1.63-1.57 (m, 2H, CH₂CH₂(CH₂)₃CH₃), 1.35-1.28 (m, 6H, CH₂CH₂(CH₂)₃CH₃), 1.25 (t, *J* = 8.0 Hz, 6H, NCH₂CH₃), 0.88 (t, *J* = 7.0 Hz, 3H, CH₂(CH₂)₄CH₃); ¹³C NMR (125 MHz, CDCl₃, 25 °C, TMS): δ = 12.4, 14.1, 22.6, 28.9, 31.5, 31.7, 35.4, 45.4, 97.0, 108.9, 110.4, 110.7, 120.3, 128.8, 131.2, 135.9, 138.9, 148.3, 152.4, 157.6, 160.8, 163.0; HRMS (EI): *m/z* calculated for C₂₆H₃₂N₂O₃[M⁺] = 420.2413; found: 420.2406.

Synthesis of Ester-Ph. To the solution of 7-(diethylamino)-2-oxo-2H-chromene-3-carboxylic acid **1** (1.25 mmol) in dry DCE, 3,5-dimethylphenol **4** (1.25 mmol), EDC (1.875 mmol) and DMAP (1.25 mmol) were added. The reaction mixture was stirred at room temperature for 12 h under argon. The mixture was diluted with water and extracted with DCM. The combined organic layers were dried over Na₂SO₄ and concentrated under reduced pressure. The crude product was purified by column chromatography (silica, hexane-ethyl acetate 1:1). Yield: 0.380g, 42%; m.p. 116-118 °C; ¹H NMR (500 MHz, CDCl₃, 25 °C, TMS): δ = 8.57 (s, 1H, CH), 7.40 (d, *J* = 9.0 Hz, 1H, Ar), 6.87 (s, 1H, Ar), 6.84 (s, 2H, Ar), 6.65 (dd, *J* = 9.0, 2.5 Hz, 1H, Ar), 6.52 (d, *J* = 2.5 Hz, 1H, Ar), 3.47 (q, *J* = 7.0 Hz, 4H, NCH₂CH₃), 2.33 (s, 6H, CH₃), 1.25 (t, *J* = 7.0 Hz, 6H, NCH₂CH₃); ¹³C NMR (125 MHz, CDCl₃, 25 °C, TMS): δ = 12.4, 21.2, 45.3, 97.0, 108.0, 108.2, 109.9, 119.4, 127.5, 131.3, 139.1, 150.0, 150.7, 153.0, 157.9, 158.7, 162.9; HRMS (EI): *m/z* calculated for C₂₂H₂₃NO₄[M⁺] = 365.1627; found: 365.1634.

Synthesis of D-Amide-Ph. The **H-Amide-Ph** (0.24 mmol, 100 mg) was dissolved in dry THF (20 ml) and to the mixture was added D₂O (3 ml). The reaction mixture was heated at 40 °C for 8 h under argon. Then the mixture was cooled to room temperature, THF was evaporated and the product was filtered.

Acknowledgements

This work was supported by the National Science Centre (Grants PRELUDIUM UMO-2017/25/N/ST5/00227 and HARMONIA 2016/22/M/ST5/00431) The authors would like to thank the National Science Centre under QuantERA programme (project 2017/25/Z/ST2/03038) and Global Research Laboratory Program (2014K1A1A2064569) through the National Research Foundation (NRF) funded by Ministry of Science, ICT & Future Planning (Korea).

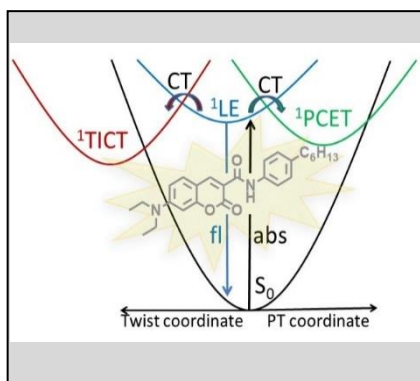
FULL PAPER

Keywords: absorption • chromophores • donor-acceptor systems • fluorescence • coumarins

- [1] M. Grätzel, *J. Photochem. Photobiol. C* **2003**, *4*, 145-153.
- [2] B. Daly, J. Ling, A. P. De Silva, *Chem. Soc. Rev.* **2015**, *44*, 4203-4211.
- [3] E. M. S. Stennett, M. A. Ciuba, M. Levitus, *Chem. Soc. Rev.* **2014**, *43*, 1057-1075.
- [4] H. B. Gray, J. R. Winkler, *Biochim. Biophys. Acta Bioenerg.* **2010**, *1797*, 1563-1572.
- [5] (a) N. V. Tkachenko, H. Lemmetyinen, J. Sonoda, K. Ohkubo, T. Sato, H. Imahori, S. Fukuzumi, *J. Phys. Chem. A* **2003**, *107*, 8834-8844; (b) N. V. Tkachenko, L. Rantala, A. Y. Tauber, J. Helaja, P. H. Hynninen, H. Lemmetyinen, *J. Am. Chem. Soc.* **1999**, *121*, 9378-9387; (c) L. Hammarström, *Acc. Chem. Res.* **2015**, *48*, 840-850; (d) L. Flamigni, B. Ventura, M. Tasiar, T. Becherer, H. Langhals, D. T. Gryko, *Chem. Eur. J.* **2008**, *14*, 169-183; (e) B. Ventura, A. Barbieri, A. Zanelli, F. Barigelletti, J. B. Seneclauze, S. Diring, R. Ziessel, *Inorg. Chem.* **2009**, *48*, 6409-6416; (f) L. Flamigni, B. Ventura, C.-C. You, C. Hippius, F. Würthner *J. Phys. Chem. C* **2007**, *111*, 622-630; (g) A. Purc, E. M. Espinoza, R. Nazir, J. J. Romero, K. Skonieczny, A. Jeżewski, J. M. Larsen, D. T. Gryko, V. I. Vullev, *J. Am. Chem. Soc.*, **2016**, *138*, 12826-12832.
- [6] R. A. Marcus, *Angew. Chem. Int. Ed.* **1993**, *32*, 1111-1121.
- [7] A. Weller, *Z. Phys. Chem.* **1982**, *133*, 93-98.
- [8] D. Gust, T. A. Moore, A. L. Moore, *Acc. Chem. Res.* **1993**, *26*, 198-205.
- [9] H. B. Gray, J. R. Winkler, *Proc. Nat. Acad. Sci.* **2005**, *102*, 3534-3539.
- [10] D. N. Beratan, J. N. Onuchic, J. R. Winkler, H. B. Gray, *Science* **1992**, *258*, 1740-1741.
- [11] G. Jones II, L. N. Lu, V. Vullev, D. J. Gosztola, S. R. Greenfield, M. R. Wasielewski, *Bioorg. Med. Chem. Lett.* **1995**, *5*, 2385-2390.
- [12] C. Shih, A. K. Museth, M. Abrahamsson, A. M. Blanco-Rodriguez, A. J. Di Bilio, J. Sudhamsu, B. R. Crane, K. L. Ronayne, M. Towrie, A. Vıcek Jr., J. H. Richards, J. R. Winkler, H. B. Gray, *Science* **2008**, *320*, 1760-1762.
- [13] M. Krzeszewski, E. M. Espinoza, C. Červinka, J. B. Derr, J. A. Clark, D. Borchardt, G. J. O. Beran, D. T. Gryko, V. I. Vullev, *Angew. Chem. Int. Ed.* **2018**, *57*, 12365-12369.
- [14] K. Rotkiewicz, K. H. Grellmann, Z. R. Grabowski, *Chem. Phys. Lett.* **1973**, *19*, 315-318.
- [15] Z. R. Grabowski, K. Rotkiewicz, W. Rettig, *Chem. Rev.* **2003**, *103*, 3899-4031.
- [16] A. Weller, *Z. Electrochem.* **1956**, *60*, 1144-1147.
- [17] A. J. Stasyuk, P. Cywiński, D. T. Gryko, *J. Photochem. Photobiol. C: Reviews* **2016**, *28*, 116-137.
- [18] J. E. Kwon, S. Y. Park, *Adv. Mat.* **2011**, *23*, 3615-3642.
- [19] J. Zhao, S. Ji, Y. Chen, H. Guo, P. Yang, *Phys. Chem. Chem. Phys.* **2012**, *14*, 8803-8817.
- [20] P. Zhou, K. Han, *Acc. Chem. Res.* **2018**, *51*, 1681-1690.
- [21] A. Brenlla, M. Veiga, J. L. Pérez Lustres, M. C. Ríos Rodríguez, F. Rodríguez-Prieto, M. Mosquera, *J. Phys. Chem. B* **2013**, *117*, 884-896.
- [22] H. Shizuka, K. Matsui, T. Okamura, I. A. Tanaka, *J. Phys. Chem.* **1975**, *79*, 2731-2734.
- [23] A. L. Sobolewski, W. Domcke, *Phys. Chem. Chem. Phys.* **2006**, *8*, 3410-3417.
- [24] T. Schultz, E. Samoilova, W. Radloff, I. V. Hertel, A. L. Sobolewski, W. Domcke, *Science* **2004**, *306*, 1765-1768.
- [25] A. L. Sobolewski, W. Domcke, *Chem. Phys. Chem.* **2006**, *7*, 561-564.
- [26] B. Valeur, M. N. Berberan-Santos, *Molecular Fluorescence Principles and Applications*, 2nd ed., Wiley-VCH Verlag & Co. KGaA, **2012**, pp. 380-384.
- [27] F. Bures, *RSC Adv.* **2014**, *4*, 58826-58851.
- [28] A. M. Moran, D. S. Egoľf, M. Blanchard-Desce, A. M. Kelley, *J. Chem. Phys.* **2002**, *116*, 2542-2555.
- [29] O. Morawski, B. Kozankiewicz, A. Miniewicz, A. L. Sobolewski, *Chem. Phys. Chem.* **2015**, *16*, 3500-3510.
- [30] Ł. Kielesiński, O. W. Morawski, Ł. Dobrzycki, A. L. Sobolewski, D. T. Gryko, *Chem. Eur. J.* **2017**, *23*, 9174-9184.
- [31] Ł. Kielesiński, D. T. Gryko, A. L. Sobolewski, O. W. Morawski, *Phys. Chem. Chem. Phys.* **2018**, *20*, 14491-14503.
- [32] A. L. Sobolewski, W. Domcke, *J. Phys. Chem. A* **2007**, *111*, 11725-11735.
- [33] M. H. V. Huynh, T. J. Meyer, *Chem. Rev.* **2007**, *107*, 5004-5064.
- [34] D. R. Weinberg, C. J. Gagliardi, J. F. Hull, C. F. Murphy, C. A. Kent, B. C. Westlake, A. Paul, D. H. Ess, D. G. McCafferty, T. J. Meyer, *Chem. Rev.* **2012**, *112*, 4016-4093.
- [35] M. Natali, S. Campagna, F. Scandola, *Chem. Soc. Rev.* **2014**, *43*, 4005-4018.
- [36] K. K. Mentel, A. Serra, P. E. Abreu, L. G. Arnaut, *Nat. Commun.* **2018**, *9*, 2903-2912.
- [37] C. F. Murphy, P. Dongare, S. C. Weatherly, C. J. Gagliardi, H. Holden Thorp, T. J. Meyer, *J. Phys. Chem. C* **2018**, *122*, 24830-24837.
- [38] E. Odella, S. J. Mora, B. L. Wadsworth, M. T. Huynh, J. J. Goings, P. A. Liddell, T. L. Groy, M. Gervaldo, L. E. Sereno, D. Gust, T. A. Moore, G. F. Moore, S. Hammes-Schiffer, A. L. Moore, *J. Am. Chem. Soc.* **2018**, *140*, 15450-15460.
- [39] N. Y. Gorobets, S. A. Yermolayev, T. Gurley, A. A. Gurinov, P. M. Tolstoy, I. G. Shenderovich, N. E. Leadbeater, *J. Phys. Chem.* **2012**, *25*, 287-295.
- [40] L. Yao, A. Grishaev, G. Cornilescu, A. Bax, *J. Am. Chem. Soc.* **2010**, *132*, 10866-10875.
- [41] N. O. C. Winter, N. K. Graf, S. Leutwyler, C. Hättig, *Phys. Chem. Chem. Phys.* **2013**, *15*, 6623-6630.
- [42] R. A. Marcus, *J. Phys. Chem.* **1989**, *93*, 3078-3086.
- [43] J. Cortes, H. Heitele, J. Jortner, *J. Phys. Chem.* **1994**, *98*, 2527-2535.
- [44] M. Bixon, J. Jortner, J. W. Verhoeven, *J. Am. Chem. Soc.* **1994**, *116*, 7349-7355.
- [45] S. Efrima, M. Bixon, *Chem. Phys.* **1976**, *13*, 447-460.
- [46] A. Kapturkiewicz, J. Herbich, J. Karpiuk, J. Nowacki, *J. Phys. Chem.* **1997**, *101*, 2332-2344.
- [47] R. A. Marcus, N. Sutin, *Biochim. Biophys. Acta* **1985**, *811*, 265-322.
- [48] C. M. Krauter, J. Mohring, T. Backup, M. Pernpointner, M. Motzkus, *Phys. Chem. Chem. Phys.* **2013**, *15*, 17846-17861.
- [49] D. Murdock, R. A. Ingle, I. V. Sazanovich, I. P. Clark, Y. Harabuchi, T. Taketsugu, S. Maeda, A. J. Orr-Ewing, M. N. R. Ashfold, *Phys. Chem. Chem. Phys.* **2016**, *18*, 2629-2638.
- [50] G. Jones II, W. R. Jackson, Ch. Y. Choi, W. R. Bergmark, *J. Phys. Chem.* **1985**, *89*, 294-300.
- [51] R. I. Cukier, D. G. Nocera, *Annu. Rev. Phys. Chem.* **1998**, *49*, 337-369.
- [52] A. Soudackov, S. Hammes-Schiffer, *J. Chem. Phys.* **2000**, *113*, 2385-2396.
- [53] (a) A. Soudackov, E. Hatcher, S. Hammes-Schiffer, *J. Chem. Phys.* **2005**, *122*, 014505; (b) G. A. Parada, Z. G. Goldsmith, S. Kolmar, B. Petterson-Rimgard, B. Q. Mercado, L. Hammarström, S. Hammes-Schiffer, J. M. Mayer, *Science* **2019**, *364*, 471-475.
- [54] S. J. Edwards, A. V. Soudackov, S. Hammes-Schiffer, *J. Phys. Chem. A* **2009**, *113*, 2117-2126.
- [55] A. Weller, *Pure Appl. Chem.* **1968**, *16*, 115-124.
- [56] B. S. Brunshwig, S. Ehrenson, N. Sutin, *J. Phys. Chem.* **1987**, *91*, 4714-4723.
- [57] H.-Y. Wu, H.-S. Ren, Q. Zhu, X.-Y. Li, *Phys. Chem. Chem. Phys.* **2012**, *14*, 5538-5544.
- [58] G. F. Manbeck, E. Fujita, J. J. Concepcion, *J. Am. Chem. Soc.* **2016**, *138*, 11536-11549.
- [59] O. Gottmann, U. Stumper, *Chem. Phys. Lett.* **1973**, *22*, 387-389.

FULL PAPER

Entry for the Table of Contents



A solvent-modulated competition between PCET and TICT processes, that both dump fluorescence of the LE state, occurs in amidocoumarins. This stems from the combination of the following facts: (1) ET occurring in excited state neutralizes the charge distribution resulting in CT state possessing low dipole moment; (2) CT state is stabilized either by proton transfer or by mutual twist of electron-donating and electron-accepting molecular moieties.

Institute and/or researcher Twitter usernames: ((optional))